

A Three-Dimensional Atomistic Kinetic Monte Carlo Study of Dynamic Solute-Interface Interaction

A T Wicaksono^{1,2}, C W Sinclair^{1,2} and M Militzer^{1,2}

¹The Centre for Metallurgical Process Engineering, The University of British Columbia, Vancouver, Canada, V6T 1Z4

²Department of Materials Engineering, The University of British Columbia, Vancouver, Canada, V6T 1Z4

E-mail: tegar@alumni.ubc.ca

Abstract. A three-dimensional atomistic Kinetic Monte Carlo model was developed and used to study the interaction between mobile solutes and a migrating interface. While the model was developed with a simplified energetic and topological description, it was also constructed to capture, in the absence of solute, the Burke-Turnbull model for interface migration and, in the presence of solutes, solute segregation to different types of interface sites. After parameterizing the model, simulations were performed to study the relationship between average interface velocity and imposed driving pressure for varying solute concentration and solute diffusivity. While the effect of solute concentration on solute drag pressure was found to be consistent with classical solute drag models, the effect of solute diffusivity was found to give a response not captured by either continuum or previously reported two-dimensional atomistic models. The dependence of maximum drag pressure on solute diffusivity was observed and attributed to the coupling between the structure of a migrating interface and the ability for solute to remain segregated to the interface.

1. Introduction

The dynamic interaction between solute atoms and migrating crystalline interfaces is crucial for determining the microstructure of many materials of technological relevance. For example, microalloying low-carbon steels with Nb promotes the formation of fine-grained ferrite resulting in an associated increase in strength and toughness [1]. Niobium in solid solution drastically retards grain boundary migration during recrystallization, and γ/α -interface migration during phase transformations [2]. Classically, this phenomenon is described at steady state by the solute drag models of Lücke-Detert [3], Cahn [4], Lücke-Stüwe [5], and Hillert [6, 7]. These continuum models predict the retardation of interface motion due to a non-equilibrium solute distribution at the interface. This distribution develops as a consequence of the competition between the solute segregation and interface migration. As pointed out by Hillert [7], the non-equilibrium solute profile leads to a dissipation of a portion of the available driving force for interface motion.

While the concept of solute drag is broadly accepted, few attempts have been made to directly evaluate the models against experimental observations, e.g. by fitting experimental data using the models in order to extract the model parameters [8–10]. One reason is that a direct comparison requires parameters that are difficult to assess experimentally. For example, the models require a knowledge of interface width, the spatial profile of solute-interface binding energy and the trans-interface solute diffusivity.

Recently, atomistic models have been used to examine the physical origins of these parameters as well as to test some of the basic assumptions of the continuum models [11, 12]. Tackling solute drag at the atomistic scale is challenging since the simulations require diffusive time scales to resolve the rate of interface migration in, for example, curvature-driven grain growth, recrystallization and diffusive phase transformations.

While molecular dynamic (MD) simulations have progressed to the point where interface velocities at the upper end of those obtained experimentally can be simulated [13], these velocities are still too high to capture velocities where solute-interface interactions are important [14]. Using the recently developed phase field crystal (PFC) technique that is capable of combining diffusive time-scales and atomistic length-scales [15], an attempt has been made to analyze solute drag problems in a non-ideal binary system [12]. Owing to computational overhead initial PFC simulations of solute drag have focused on two-dimensional domains. In a first approximation, the results reported from PFC simulations are consistent with Cahn’s solute drag model.

One of the most commonly employed simulation tools for tackling problems that involve atomistic length-scales and diffusive time-scales is atomistic kinetic Monte Carlo (aKMC). Mendelev et al [11, 16] applied this technique to study the migration of a driven interface in a two-dimensional, binary system where solute drag in a non-ideal solid solution was examined. Departures from continuum models were observed, notably an asymmetric effect between attractive and repulsive solute-interface interaction on the drag pressure was reported [11]. While these simulations provide valuable insights into possible atomic scale contributions missed in the classic continuum solute drag models, the limitation to two-dimensions and simplified energetics limit the generality of the conclusions that can be drawn.

In the work presented here, atomistic kinetic Monte Carlo simulations of solute drag have been extended to three dimensions. The paper is organized as follows. First, the model is presented starting from a description of the interface structure. The energetics and kinetics of the system are described next. The simulation results are then discussed and finally evaluated in the context of the continuum Cahn model [4].

2. Simulation Methodology

2.1. Geometry and energetics of a single component bicrystal

The approach adopted here has been to focus on developing a model that captures many of the basic features of a migrating crystalline interface interacting with mobile solute atoms without capturing the crystallographic detail of the interface itself. To do this, the simulation box was constructed from a single body centered cubic (BCC) crystal containing $N_X \times N_Y \times N_Z$ unit cells. The box height N_Z is 200 unit cells, chosen such that a steady state interface motion can be observed. The width N_X and length N_Y were systematically increased to determine the critical temperature for roughening transition [17]. All subsequent simulations were conducted in a system with $N_X = N_Y = 120$ unit cells where the finite-size effect, as indicated by the relative increase of interface roughness at a given temperature with increasing system size, was found to be no longer significant, i.e. a less than 10% change.

In this construction, rather than being defined as the region separating two crystals having different orientations, an interface was constructed from a domain having a single crystallographic orientation by assigning a ‘spin’ to each atom. The atoms in one half of the bicrystal were assigned a ‘spin’ of $+\frac{1}{2}$ (dark-coloured atoms in Figure 1) while those in the other half of the box were assigned a ‘spin’ of $-\frac{1}{2}$ (light-coloured atoms in Figure 1). Interfacial atoms are those who have at least one nearest neighbour that belongs to the other grain. One can envision this as a coherent interface separating two crystals having the same orientation and lattice parameter, but not necessarily the same energy. Periodic boundary conditions were applied to the simulation walls perpendicular to the interface plane, while a toroidal boundary condition was applied to the walls parallel to the interface plane [16]. These boundary conditions ensure that the simulation box contains only one interface plane.

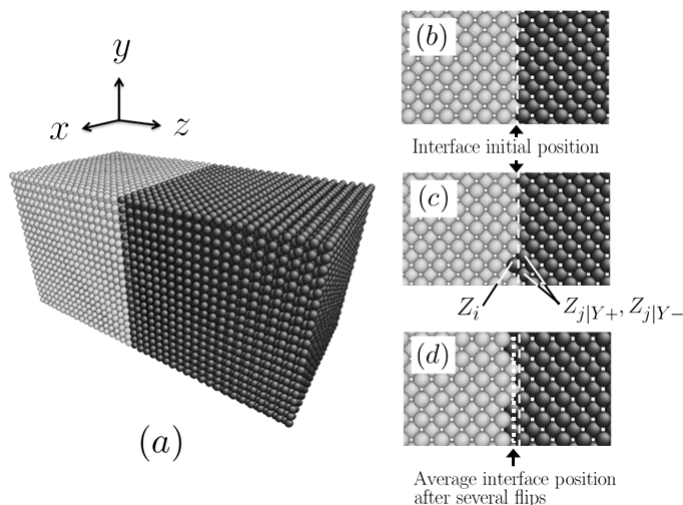


Figure 1. (a) A typical simulation box where two crystals of the same orientation are separated by a flat $\{001\}$ interface, (b) The initial position of the interface, (c) A flipping event occurred at the spin i whose neighbours are j , (d) The average position of the interface advances upon several flipping events of the spins belonging to one of the grains.

Coinciding with this simplified interfacial structure, a simplified mechanism of interface migration was also adopted. Only solvent atoms residing at the interface plane (Figure 1(b)) can flip their membership from their current grain to the adjacent grain by switching their spin, effectively shifting the average position of the interface, see Figure 1(d). The rate of these flipping events for a given atom is assumed to depend on its local environment. Without an energy bias between the two crystals, the flipping events occur randomly to both the left and right. This results in an interface that roughens but whose average position remains the same. If, however, one of the crystals is assumed to have a higher energy than the other, flipping will be biased in one direction causing the interface to migrate.

Taking the energy of a system containing a flat interface as a reference, the excess energy associated with a non-flat interface is assumed to be [18],

$$E_{\text{pure}} = \gamma \sum_{i=1}^{N_X N_Y} \sum_{j=1}^4 (Z_i - Z_j)^2 \quad (1)$$

In this description, similar to the Discrete Gaussian Solid on Solid (DGSOS) model [19], the excess energy of a rough interface is characterized by a set of half-integral multiple of lattice parameter Z_i indicating the position along z-direction of an interfacial atom of a given spin from an arbitrary XY-plane of reference, here taken as the initial interface position. The excess energy is given by the sum of the square of the differences between the height of each atom Z_i and those of adjacent interfacial atoms j , $Z_{j|X+}$, $Z_{j|X-}$, $Z_{j|Y+}$ and $Z_{j|Y-}$, where i and j belong to the same type of spin (see Figure 1(c)). The magnitude of the energy penalty due to roughening is scaled by γ , which can be thought of as an effective surface energy with units of energy per unit area.

2.2. Introducing solutes: energetics and interaction with interface

From the single component bicrystal described above, binary alloys were constructed having solute atoms residing in octahedral interstitial sites of the BCC lattice. We have assumed identical behaviour for solute in the two grains, with no solute-solute interactions.

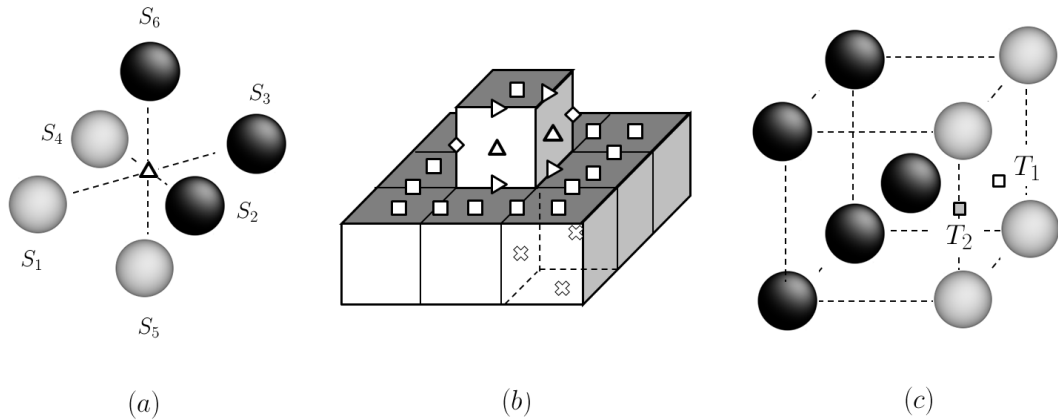


Figure 2. (a) An octahedral site in a BCC lattice surrounded by its six neighbouring solvent atoms, (b) Different types of octahedral site as defined by Equation (2), see also Table 1, (c) Two multiplicities of terrace site ($\omega = 1.0$) found in a flat interface.

The interaction between solute atoms and the interface were designed such that the solute prefers to sit in positions where it is surrounded by solvent atoms from both sides of the interface. An octahedral site is surrounded by six solvent atoms, which we pair into three groups: $(S_1 : S_3)$, $(S_2 : S_4)$ and $(S_5 : S_6)$, see Figure 2(a), the midpoint of each being the octahedral site itself. The total energy of the system is modified when a solute atom occupies a site that separates two solvent atoms belonging to different grains. Using this convention a bulk octahedral site is defined as one surrounded entirely by solvent atoms from the same grain. The energy of non-bulk sites are scaled based on the parameter ω , where

$$\omega = 0.5 (|S_1 - S_3| + |S_2 - S_4| + 2|S_5 - S_6|) \quad (2)$$

with $S_i = \pm 0.5$ (for left/right grain)

Based on Equation (2), five distinct types of octahedral sites can be identified. The factor two in the third term of Equation (2) is included to ensure that the two types of octahedral site found in a perfectly flat interface (T_1 on the face center and T_2 on the edge midpoint, see Figure 2(c)) have $\omega = 1$. The values of ω and their multiplicity for the five types of sites are listed in Table 1.

Table 1. Types of interstitial octahedral sites and their ω -values, see Equation (2).

| Symbol | Site Type | ω -values | Multiplicity |
|------------------|-----------|------------------|--------------|
| \times | Bulk | 0.0 | 2 |
| \triangleright | Ledge | 0.5 | 3 |
| \square | Terrace | 1.0 | 3 |
| \diamond | Kink | 1.5 | 1 |
| \triangle | Island | 2.0 | 1 |

The binding energy of solute to an octahedral site is assumed to be proportional to its ω -value and is given by $E_{\text{bind}} = -\varepsilon_{\text{B}}\omega$. Here, ε_{B} is the binding energy to a site in a flat interface, a positive value of which indicating an attractive solute-interface interaction.

2.3. Kinetics of interface migration and solute diffusion

The system dynamics were simulated using a classic kinetic Monte Carlo scheme where the kinetics are dictated by changes in the total energy of the system before and after an event occurs [20, 21]. In a bicrystal containing solute, the total system energy relative to a solute-free system containing a flat interface is

$$E = E_{\text{pure}} + E_{\text{solute-interface}} = \left(\gamma \sum_{i=1}^{N_x N_y} \sum_{j=1}^4 (Z_i - Z_j)^2 \right) + \left(-\varepsilon_{\text{B}} \cdot \sum_{l=1}^{6N_x N_y N_z} \omega_l \phi_l \right) \quad (3)$$

where the summation index l is over all octahedral sites and ϕ denotes the occupancy of site l , i.e. one if occupied and zero otherwise. A fast-searching algorithm [22] was implemented along with the residence time method [23].

The rates of two fundamental events have to be considered in this model: the switching of interfacial atoms from one grain to the other and solute diffusion. In the simplest case, the former is taken to occur with a rate,

$$\Gamma_{\text{int}} = \nu \cdot \exp\left(-\frac{Q_{\text{m}} + \Delta E/2}{kT}\right) \quad (4)$$

where ν is the attempt frequency, Q_{m} is the activation barrier for interface migration and ΔE is the difference between the total energy of the system before and after the event, k is the Boltzmann constant and T is the absolute temperature [20, 21]. The energy change ΔE in this case arises from changes of interfacial energy, via $(Z_i - Z_j)$ from the first term in Equation (3), as well as changes in the number of occupied non-bulk octahedral sites due to the interface motion away from segregated solutes, via ω_l from the second term in Equation (3).

Under these conditions, the average position of the interface will fluctuate around its initial average position. To drive the interface in one direction, a difference between the energy of solvent atoms belonging to the two grains must be imposed. This is done by raising the energy of solvent atoms on one side of the interface by an amount of $P\Omega$, P being the driving pressure and Ω the atomic volume. The rate of flipping in one direction is then still governed by Equation (4) while the rate of flipping in the other direction is given by

$$\Gamma_{\text{int-reverse}} = \nu \cdot \exp\left(-\frac{Q_{\text{m}} + P\Omega + \Delta E/2}{kT}\right) \quad (5)$$

Written in this way, the rate of interface migration for a pure system obeys the classic Burke-Turnbull relationship [24]. This approximates to a linear dependence between P and interface velocity at low driving pressures, but more generally to a non-linear relationship at high driving pressures where the velocity approaches a limiting value. This contrasts with the interface migration model in [16] where the velocity increases exponentially with P .

The second rate that has to be captured is that associated with solute diffusion. The rate of solute hops from one octahedral site to the next is governed by,

$$\Gamma_{\text{solute}} = \nu \cdot \exp\left(-\frac{Q_{\text{d}} + \Delta E/2}{kT}\right) \quad (6)$$

where Q_{d} is the activation barrier for bulk solute diffusion and the energy change ΔE in this case comes only from changes in the occupancy parameter ϕ from the second term of Equation (3). Based on the above description, the model has been parameterized using values that are consistent with those expected in metallic alloys. Table 2 summarizes the definition and the values of all fixed parameters chosen for simulations. Parameters that will be varied during simulations are the driving pressure P , the activation barrier for bulk solute diffusion Q_{d} , the absolute temperature T and the solute concentration C_0 .

Table 2. Basic simulation parameters.

| Parameter | Definition | Values |
|--------------------------|---|--|
| a | Lattice parameter | 0.3 nm |
| γ | Surface energy | 52.8 mJ/m ² |
| ε_{B} | Binding energy of solute to the interface | 0.17 eV |
| ν | Attempt frequency | 10 ¹³ s ⁻¹ |
| Ω | Atomic volume | 2.7 × 10 ⁻²⁹ m ³ |
| Q_{m} | Activation energy for interface migration | 0.1 eV |

3. Results

3.1. Interface migration in a solute-free bicrystal

As a starting point for our investigations, simulations were performed to establish the behaviour of the system in the absence of solute. As has been previously reported for similar DGSOS models [19], the interface undergoes a roughening transition at a critical temperature T_c . Identifying this transition is important since the temperature at which the interface operates relative to T_c determines its structure and thus its dynamics. To determine T_c , a series of simulations were performed at different temperatures and different system sizes with a fixed surface energy $\gamma = 52.8$ mJ/m². The structure of the interface was monitored via the time-average of its roughness R [17],

$$R = \left(\frac{1}{N_X N_Y - 1} \sum_{i=1}^{N_X N_Y} (Z_i - \bar{Z})^2 \right)^{1/2} \quad (7)$$

where \bar{Z} is the average interface position.

Using the finite-size scaling method [25] T_c was found to be approximately $kT_c/a^2\gamma \sim 2.42$, corresponding to $T_c = 833$ K for the surface energy and lattice parameter in Table 2. Below T_c , the interface remains relatively flat, consisting predominantly of terrace octahedral sites.

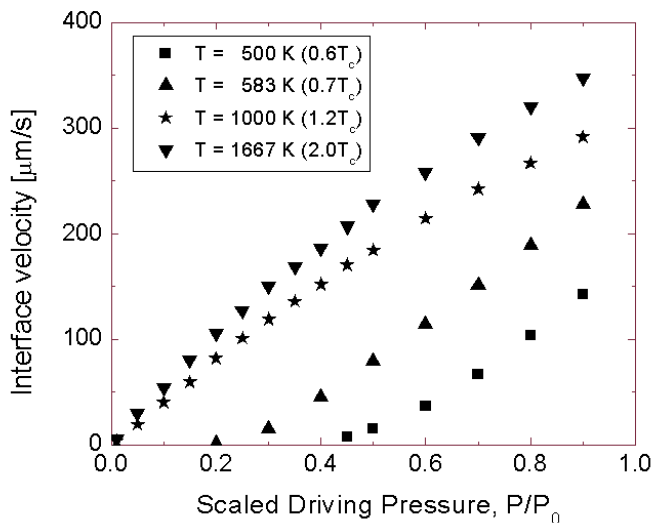


Figure 3. Dependence of average interface velocity on imposed driving pressure (P) for a solute-free system with $\gamma = 52.8$ mJ/m². The driving pressure is scaled by $P_0 = kT/\Omega$.

Figure 3 illustrates the dependence of average interface velocity on the imposed driving pressure P for temperatures above and below the critical temperature. The average interface velocity was obtained at a given temperature by obtaining the slope of a linear fit to the average interface position (\bar{Z}) as a function of time. Each point on this plot represents the average of five different simulations, the variation between runs being smaller than the size of the symbols in this figure.

At $T < T_c$, the interface motion is determined by a two-step process of nucleation of an island, e.g. the atom i in Figure 1(c), followed by lateral propagation of ledges surrounding the nucleated island. Owing to the high barrier for island nucleation relative to kT , the rate of interface migration at low temperatures and low driving pressures is negligibly small. In order to have a significant motion of the interface, a critical driving pressure has to be applied, its magnitude increasing with decreasing temperatures.

At $T \geq T_c$, the barrier for island nucleation is reduced relative to kT and the interface migrates predominantly by spatially uncorrelated island nucleations. The interface roughens and the velocity-driving pressure relationship obeys the Burke-Turnbull model, where for sufficiently small driving pressures the relationship is approximately linear [24].

Based on the above results, all subsequent simulations were performed at $T = 1000$ K $> T_c$ so as to allow for a direct comparison with predictions from continuum models, where a linear velocity-driving pressure relation is typically assumed in the low driving pressure limit.

3.2. Interface migration in the presence of diffusing solutes

In all simulations involving binary alloys, the system was populated with a random distribution of solute. A driving pressure was next imposed and the interface was observed to migrate. A transient regime ensued until a steady-state distribution of solute segregated to the interface was achieved. Upon reaching steady-state, the average interface displacement was found to vary linearly with time, as in the case of simulations of the single-component bicrystals described above.

Both solute concentration and solute diffusivity were varied to study their effect on the rate of interface migration. The effect of solute concentration on interface migration is shown in Figure 4 for a solute diffusion characterized by $Q_d = 0.27$ eV. At low driving pressures one observes that the interface velocity decreases with solute concentration for a given driving pressure. As the driving pressure is increased, the interface velocity of the alloy system approaches that of the solute-free system, indicating a breaking-away of the interface from its solute cloud. This qualitatively obeys the classical description of solute drag from the continuum models discussed earlier (see e.g. [4]).

Following Cahn [4] and based on the results shown in Figure 4(a), the drag pressure was computed as the difference in driving pressure required to achieve the same velocity in the solute-containing and solute-free system. For the solute-free system the velocity-driving pressure relationship was fit to the Burke-Turnbull model, $V = V_T (1 - \exp(-P/P_T))$ [24] where (V_T, P_T) were taken to be temperature-dependent parameters with $V_T = 553$ $\mu\text{m/s}$ and $P_T = 623$ MPa at 1000 K. A linear regime of velocity-driving pressure was observed for sufficiently low driving pressures, i.e. $P \leq 0.3P_T \approx 200$ MPa.

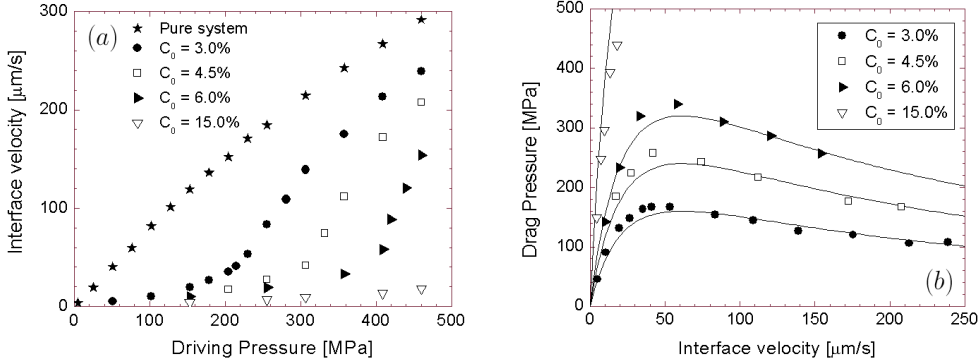


Figure 4. (a) Interface velocity as a function of imposed driving pressure for systems containing different concentration of solute with $Q_d = 0.27$ eV, (b) Drag pressure calculated and plotted versus velocity based on data in (a). The solid curves were drawn using Equation (8) with $\alpha = 348 \text{ MPa}(\mu\text{m/s})^{-1}$ and $\beta = 1.63 \times 10^{-2} (\mu\text{m/s})^{-1}$.

The calculated drag pressure P_D is shown in Figure 4(b) and compared with a continuum model that is given by,

$$P_D = \frac{\alpha C_0 V}{(1 + \beta V)^2} \quad (8)$$

where α and β are the model parameters. The model in Equation (8) varies subtly from the one originally proposed in [4] and the origin of this expression is outlined in Appendix A.

The aKMC results in Figure 4(b) are well described by this expression using a single set of parameters $\alpha = 348 \text{ MPa}(\mu\text{m/s})^{-1}$ and $\beta = 1.63 \times 10^{-2} (\mu\text{m/s})^{-1}$, consistent with the fact that both are expected to be independent of solute concentration [4]. While Cahn provided the explicit forms of α and β , both being a function of the interface width, the diffusivity profile and the binding energy profile, none of these are easily extracted from the present simulations. Therefore, α and β have been treated as adjustable parameters.

While the aKMC results and the Cahn's model agree when the role of solute concentration is considered, the same cannot be said when the effect of solute diffusivity on solute drag is examined. Figure 5(a) illustrates the velocity-driving pressure and drag pressure-velocity relationships for systems having $C_0 = 3.0$ at% and different solute diffusivities. Continuum solute drag models predict that these curves would collapse when the interface velocity is scaled by the solute diffusivity and a characteristic length-scale, typically taken to be the interface width [4]. Scaling the data in this way (Figure 5(b)) does not appear to bring the normalized velocity at peak drag pressure into coincidence. The continuum models would also predict that the peak drag pressure should be independent of the solute diffusivity. Instead, Figure 5(b) reveals that the peak drag pressure increases with solute diffusivity.

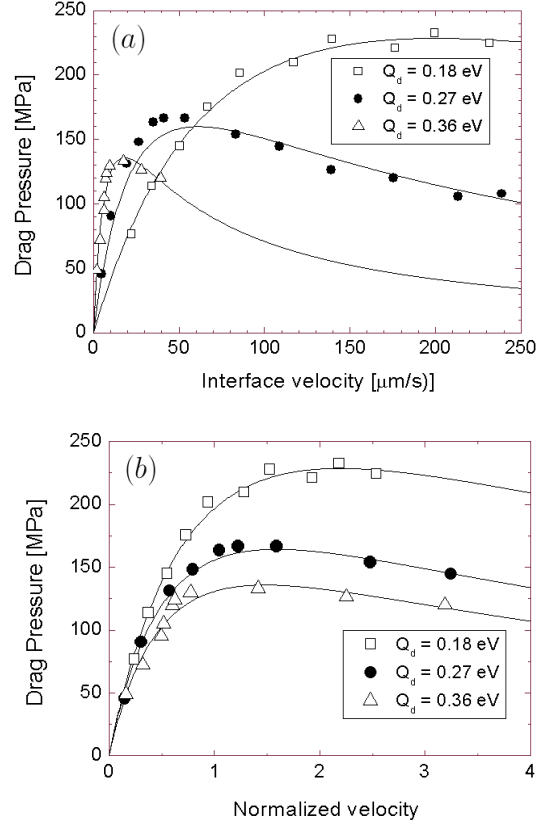


Figure 5. Drag pressure versus (a) velocity, and (b) normalized velocity for systems containing 3 at% solute and different solute diffusivities. The normalized velocity is the velocity multiplied by the ratio of lattice parameter and diffusivity. Solid lines indicate the empirical fit between simulation results and empirical model, Equation (8).

The deviation from classical continuum model can be attributed to the fluctuation of interface topology during the course of its migration. Observing the structure of the interface at the velocity corresponding to the peak drag pressure reveals significant differences between systems containing slow diffusing and fast diffusing solute. Figure 6 illustrates snapshots of the interface plane under these conditions, particularly highlighting the roughness of the interface plane. While the interfaces exhibit some similarities, one can see that the interface interacting with fast diffusing solute exhibits a higher degree of spatial correlation in the interface ‘height’ leading to local bulging in several locations. Such bulges require the coordinated motion of a large number of neighbouring interface segments, suggesting a correlation of the local behaviour of interfacial atoms.

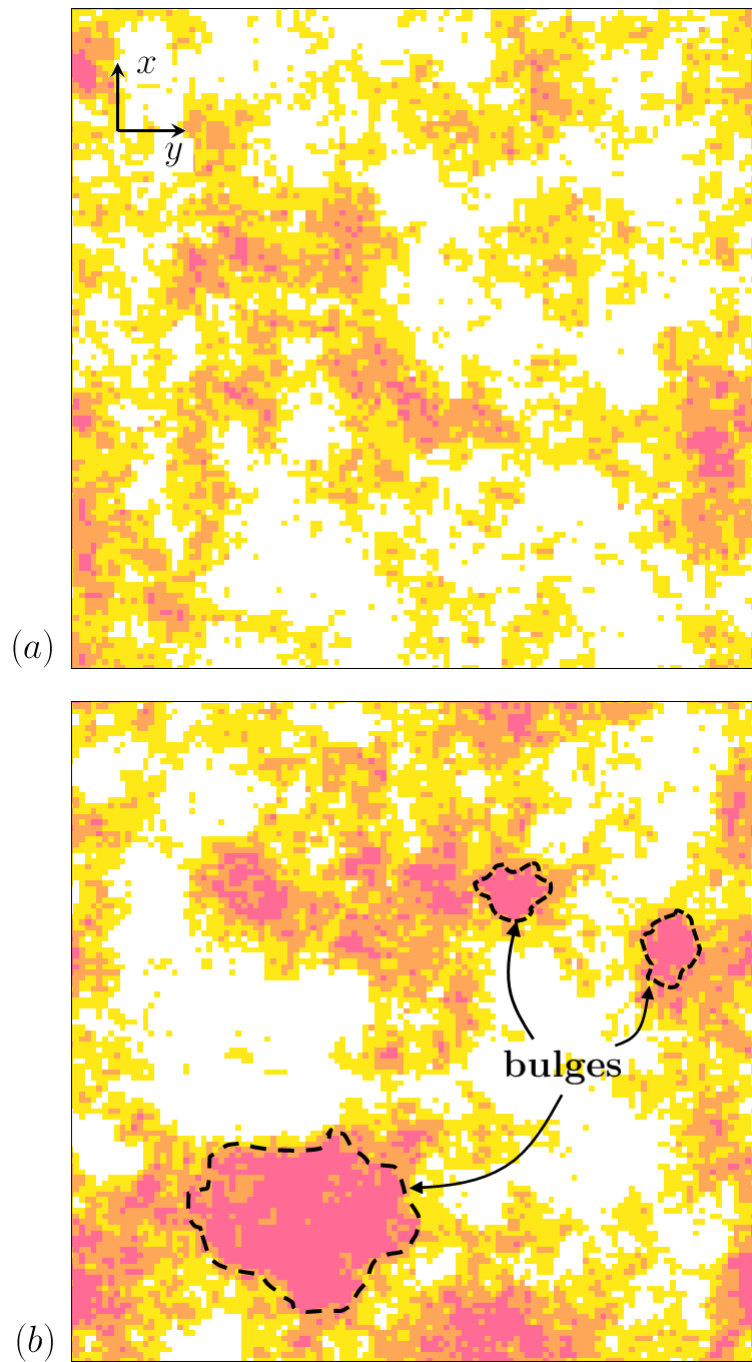


Figure 6. Snapshots of interface cross-sectional view during its steady-state migration at the velocity corresponding to maximum drag pressure and interacting with (a) slow-diffusing solute and (b) fast-diffusing solute. Yellow pixels indicate interfacial solvent atoms i whose z -position is equal to the average position of the interface ($Z_i = \bar{Z}$). White, orange and salmon pixels indicate $Z_i = \bar{Z} - a$, $Z_i = \bar{Z} + a$ and $Z_i > \bar{Z} + a$, respectively. Regions corresponding to bulges in (b) are highlighted.

As illustrated in Figure 7(a), this behaviour can be further quantified by examining the interface roughness R from each data point in Figure 5(b).

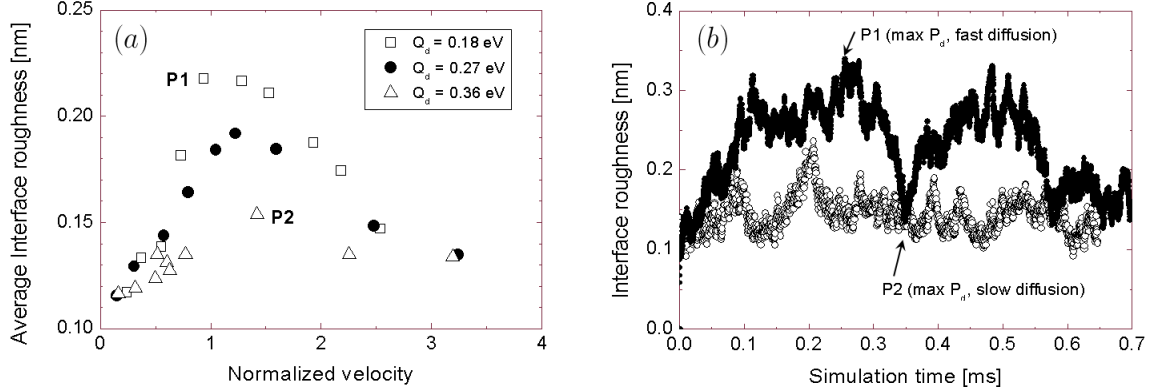


Figure 7. (a) The time-average interface roughness (Equation (7)) plotted against the normalized interface velocity, i.e. velocity \times flat interface width/bulk diffusivity, for varying solute diffusivity; (b) A time-resolved trace of interface roughness corresponding to the peak drag pressure for interface interacting with fast-diffusing (filled circles) and slow-diffusing solutes (open circles), i.e. point P1 and P2 in (a).

At low and high interface velocities, the interface remains relatively flat irrespective of solute diffusivity, its roughness being similar to that of a non-driven interface. In the case of systems containing slow diffusing solutes, the interface roughness increases by less than half its stationary value as the velocity approaches its value at the peak drag pressure. In the case of fast-diffusing solute, the interface roughness nearly doubles relative to its stationary value. A direct consequence of the interface motion in the presence of fast diffusing solute is a higher rate of energy dissipation, resulting in a higher peak drag pressure.

While this provides an explanation for the observed increase of maximum drag pressure with increasing solute diffusivity, it does not explain the relationship between solute diffusivity and interface topology. The dependence of interface topology on solute diffusivity can be explained from the perspective of the rate of solute hopping into and away from a migrating interface.

For a detailed discussion about this phenomenon, one may start by considering a flat interface containing a steady-state distribution of segregated solute. At some location along the flat interface plane, a small interface segment will advance into the adjacent crystal due to the applied driving pressure. The next atomistic event depends sensitively on the diffusivity of the solute atoms surrounding this advanced interface segment.

At low diffusivity (high Q_d), the rate of solute hopping is predominantly determined by the activation barrier Q_d , the rate of hopping to and from the interface being approximately the same, i.e. $\Gamma_{\text{bulk} \rightarrow \text{int}}^{\text{sol}} \approx \Gamma_{\text{int} \rightarrow \text{bulk}}^{\text{sol}} = \nu \exp(-Q_d/kT)$ since Q_d is relatively large compared to ϵ_B . The next event in the simulation is also likely to be the advance of an adjacent interface segment. This is due to the imposed driving pressure that favours this event as well as the fact that the system energy can be lowered by preferentially having the neighbouring segments to advance. This operation is expected to repeat along the interface plane to reduce the total interface energy (Equation (3)), occurring more frequently than solute atoms diffusing into the sites available in the advanced interface

segments. The distribution of interface height is thus expected to be largely uncorrelated as seen in Figure 6(a). Moreover, it is unlikely that an advanced interface segment will further proceed before the neighbouring segments catch up because of the increased roughening penalty, see Equation (1).

If the solute diffusivity is very high (low Q_d), however, then immediately after the interface segment advances the solute atom left behind has a high probability to jump back to a location in the (now advanced) interface since the barrier for jumps into the interface is significantly lowered by the binding energy of the solute to the interface, $\Gamma_{\text{bulk} \rightarrow \text{int}}^{\text{sol}} \approx \nu \exp(-(Q_d - 0.5\varepsilon_B)/kT)$. The rates of solute jumping out of the interface, on the other hand, are low owing again to the binding energy of solute to the interface, i.e. $\Gamma_{\text{int} \rightarrow \text{bulk}}^{\text{sol}} \approx \nu \exp(-(Q_d + 0.5\varepsilon_B)/kT)$. Segregation of solute to a bulge on the interface will result in a reduction in the total system energy, partially compensating for the increased energy due to the larger total area of the interface. In this situation, the next event can include a further extension of the already advanced interface under the imposed driving pressure since the energy penalty associated with this event is partially compensated by the segregated solute. This is evident in Figure 6(b) where the height distribution appears more spatially correlated compared to Figure 6(a). The advance of a single interfacial atom by more than two atomic positions ahead of its neighbours in the same grain has a low probability owing to the rapid increase in interfacial energy (Equation 1). When a bulge extends beyond this point, its growth will stall and the interface will flatten so as to reduce the total energy of the system. Based on this explanation and as observed in simulations (Figure 7(b)), bulges will appear, grow then slow down and finally disappear as the whole interface advances with new bulges appearing at other locations on the interface plane.

These results reveal a phenomenon that neither two-dimensional simulations [11, 12] nor continuum models have previously revealed [4]. The spatial degree of freedom available for the structural fluctuation of a two-dimensional interface allow for a more complex interfacial topography than the topographies reported in two dimensional systems. While this leads to a non-classical dependence of the peak drag pressure on solute diffusivity, it has to be emphasized that, otherwise, the results presented here semi-quantitatively follow the predictions of the classical solute drag models [3–5]. In some regards it is surprising that an effect of the interface structure, arising explicitly from the different types of sites for solute at the interface, was not found to play a significant role in results even though the population of these different types of sites changes depending on the topology (e.g. roughness) of the interface.

Based on the ability of the Cahn’s solute drag model to capture the trends in terms of velocity-driving pressure, it is concluded that the use of an effective binding energy is sufficient to describe the solute drag effect observed here. A natural question that arises from this is how best to compute such an effective binding energy profile based on a discrete atomistic model. Similarly, quantities such a trans-interface diffusivity and interface width do not have natural analogues in atomistic simulations [12, 26]. Given that the parameters α and β in the Cahn model depend on these quantities, it is not possible to make a fully quantitative comparison with atomistic simulations. Here, for example, α and β have had to be treated as adjustable parameters. These simulation results, however, may be used to develop useful ways of finding effective parameters, e.g. the interface width, when modelling experimental data.

Finally, one must recognize the simplicity of the energetic and topological descriptions of the solute-interface interactions employed here. These descriptions limit the possible interface configurations being simulated. Further simulations using more realistic interface/solute topology and interactions need to be investigated to test the generality of these findings and to extend the results to less idealized alloy systems.

4. Summary

An atomistic Kinetic Monte Carlo model has been developed having a simplified description of system energy and interface topology. Using this model the effect of diffusing solute on a migrating interface has been investigated. The results are in semi-quantitative agreement with the predictions of continuum models, though a departure from these classic models was observed when the effect of solute diffusivity on interface migration was examined. Unlike the classic models which predict the peak drag pressure to be independent of solute diffusivity, the simulations reported here showed an increasing peak drag pressure with solute diffusivity. It was shown that this effect arises from a change in the roughness of the interface at the peak drag pressure depending on the solute diffusivity. Fast diffusing solutes allow for local bulges to form and then disappear on the interface plane during the interface migration. The formation of these bulges results in a more tortuous path for interface migration and therefore a higher rate of energy dissipation during migration. A fully quantitative comparison with Cahn's solute drag model is limited by the fact that the model parameters, such as binding energy profile, trans-interface diffusivity and interface width, do not have one-to-one correspondence in the atomistic simulations.

Acknowledgments

The authors thank the Natural Sciences and Engineering Research Council of Canada (NSERC) for financial support. Valuable discussions with Michael Greenwood and Michel Perez are gratefully acknowledged.

Appendix A. Modified solute drag model

Cahn's solute drag model [4] was developed by coupling a steady-state diffusion equation,

$$C'' + \left(\varepsilon'_B + \frac{D'}{D} + \frac{V}{D} \right) C' + \left(\frac{D'}{D} \varepsilon'_B + \varepsilon''_B \right) C = 0 \quad (\text{A.1})$$

whose solution $C(x)$ requires assumptions about the spatial profile of solute diffusivity $D(x)$ and the interfacial binding energy $\varepsilon_B(x)$, to an expression for the drag pressure based on the force exerted by each solute atom on the interface,

$$P_D = -\frac{1}{\Omega} \int_{-\infty}^{+\infty} (C(x) - C_0) \varepsilon'_B dx \quad (\text{A.2})$$

While this coupled system of equations can be solved analytically in the limit of low or high velocity, a completely general, closed form expression for the drag pressure is not available. Cahn proposed an expression to approximately merge responses obtained in the high and low velocity limit. Cahn's proposed expression was [4]

$$P_D = \frac{\alpha C_0 V}{1 + (\beta V)^2} \quad (\text{A.3})$$

When Equation (A.1) assumes a constant diffusivity and a triangular binding energy profile, explicit forms of α and β were available [4]. In this case, the original model (Equation (A.3)) is shown to fit well the drag pressure obtained from numerically solving coupled Equations (A.1) and (A.2). If a non-uniform diffusivity profile is assumed, e.g. the case where the trans-interface

diffusivity is different from the bulk diffusivity, the original model (Equation (A.3)) does not fit the numerical solution as well, see the dashed curve in Figure A1. A similar trend is also observed when the original model (Equation (A.3)) is used to fit the numerical solutions to the modified diffusion equation similar to Equation (A.1) that includes site-saturation correction [5]. The parameters (α, β) used to draw the dashed curve in Figure A1 were calculated from the slope and the ordinate intercept of linear regression V^2 versus V/P_D where (V, P_D) are the points obtained from numerically solving coupled Equations (A.1) and (A.2).

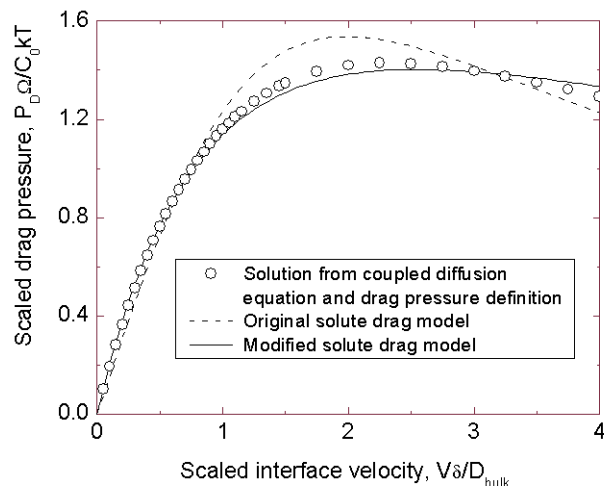


Figure A1. The drag pressure-velocity trend from solving coupled Equations (A.1) and (A.2) that employ a non-uniform diffusivity profile is fitted using Cahn’s original model, Equation (A.3), and the model proposed in this work, Equation (8). Both the diffusivity and the binding energy spatial profile are triangular where $D(x \leq -\frac{\delta}{2}, x \geq +\frac{\delta}{2}) = D_{\text{bulk}}$, $D(x = 0) = D_{\text{interface}} = 4D_{\text{bulk}}$, $\varepsilon_B(x \leq -\frac{\delta}{2}, x \geq +\frac{\delta}{2}) = 0$ and $\varepsilon_B(x = 0) = -2kT$.

The models’s inability to fit the data points relies on the fact that the regression form mentioned earlier showed a parabolic instead of linear trend. A slight modification to the model, Equation (8), was proposed and it was found that this modified model fits the numerical solution reasonably well, see the solid curve in Figure A1. Consistent with the fact that the present simulations involve a diffusivity into and within the interface that are affected by the solute-interface binding energy, it is found that the modified model also gives a better match to the simulation results compared to the original model above.

References

- [1] Deardo A J 2003 *Int. Mater. Rev.* **48** 371–402
- [2] Cuddy L J 1982 *Thermomechanical Processing of Microalloyed Austenite* (TMS-AIME)
- [3] Lücke K and Detert K 1957 *Acta Metall.* **5** 628–637
- [4] Cahn J W 1962 *Acta Metall.* **10** 789–798

- [5] Lücke K and Stüwe H P 1971 *Acta Metall.* **19** 1087–1099
- [6] Hillert M 1975 *Met. Trans. A* **6** 5–19
- [7] Hillert M 2004 *Acta Mater.* **52** 5289–5293
- [8] Zurob H S, Zhu G, Subramanian S V, Purdy G R, Hutchinson C R and Bréchet Y 2005 *ISIJ International* **45** 713–722
- [9] Sinclair C W, Hutchinson C R and Bréchet Y 2007 *Metall. Mater. Trans. A* **38** 821–830
- [10] Hutchinson C R, Zurob H S, Sinclair C W and Bréchet Y 2008 *Scr. Mater.* **59** 635–637
- [11] Mendeleev M I and Srolovitz D J 2002 *Modell. Simul. Mater. Sci. Eng.* **10** R79–R109
- [12] Greenwood M, Sinclair C W and Militzer M 2012 *Acta Mater.* **60** 5752–5761
- [13] Deng C and Schuh C A 2011 *Phys. Rev. B* **84** 214102
- [14] Mishin Y, Asta M and Li J 2010 *Acta Mater.* **58** 1117–1151
- [15] Greenwood M, Rottler J and Provatas N 2011 *Phys. Rev. E* **83** 031601
- [16] Mendeleev M I, Srolovitz D J and E W 2001 *Phil. Mag. A* **81** 2243–2269
- [17] Olmsted D L, Foiles S M and Holm E A 2007 *Scr. Mater.* **57** 1161–1164
- [18] Weeks J D and Gilmer G H 1979 *Adv. Chem. Phys.* **40** 157–228
- [19] Lapujoulade J 1994 *Surf. Sci. Rep.* **20** 191–249
- [20] Rautiainen T T and Sutton A P 1999 *Phys. Rev. B* **59** 13681–13692
- [21] Van der Ven A, Ceder G, Asta M and Tepeesch P D 2001 *Phys. Rev. B.* **64** 184307
- [22] Blue J L, Beichl I and Sullivan F 1995 *Phys. Rev. E* **51** R867–R868
- [23] Fichthorn K A and Weinberg W H 1991 *J. Chem. Phys.* **95** 1090–1096
- [24] Burke J and Turnbull D 1952 *Prog. Met. Phys.* **3** 220–292
- [25] Landau D P and Binder K 2005 *A Guide to Monte Carlo Simulations in Statistical Physics, 2nd edition* (Cambridge University Press)
- [26] Mendeleev M I, Srolovitz D J, Ackland G J and Han S 2005 *J. Mater. Res.* **20** 208–218